energies

MDPI

Article

Multi-Objective Optimization of a Small-Scale ORC-VCC System Using Low-GWP Refrigerants

Łukasz Witanowski

Institute of Fluid-Flow Machinery, Polish Academy of Sciences, 80-231 Gdańsk, Poland; lwitanowski@imp.gda.pl

Abstract: The increasing global demand for energy-efficient cooling systems, combined with the need to reduce greenhouse gas emissions, has led to growing interest in using low-GWP (global warming potential) refrigerants. This study conducts a multi-objective optimization of a small-scale organic Rankine cycle–vapor compression cycle (ORC-VCC) system, utilizing refrigerants R1233zd, R1244yd, and R1336mzz, both individually and in combination within ORC and VCC systems. The optimization was performed for nine distinct cases, with the goals of maximizing the coefficient of performance (COP), maximizing cooling power, and minimizing the pressure ratio in the compressor to enhance efficiency, cooling capacity, and mechanical reliability. The optimization employed the Non-dominated Sorting Genetic Algorithm III (NSGA-III), a robust multi-objective optimization technique that is well-suited for exploring complex, non-linear solution spaces. This approach effectively navigated trade-offs between competing objectives and identified optimal system configurations. Using this multi-objective approach, the system achieved a COP of 0.57, a pressure ratio around 3, and a cooling capacity exceeding 33 kW under the specified boundary conditions, leading to improved mechanical reliability, system simplicity, and longevity. Additionally, the system was optimized for operation with a cooling water temperature of 25 °C, reflecting realistic conditions for contemporary cooling applications.

Keywords: waste heat; multi-objective optimization; organic Rankine cycle; vapor compression cycle; Non-dominated Sorting Genetic Algorithm III

check for updates

Citation: Witanowski, Ł. Multi-Objective Optimization of a Small-Scale ORC-VCC System Using Low-GWP Refrigerants. *Energies* **2024**, *17*, 5381. https://doi.org/10.3390/en17215381

Academic Editor: Artur Blaszczuk

Received: 4 October 2024
Revised: 25 October 2024
Accepted: 28 October 2024
Published: 29 October 2024

Copyright: © 2024 by the author. Licensee MDPI, Basel, Switzerland. This article is an open access article distributed under the terms and conditions of the Creative Commons Attribution (CC BY) license (https://creativecommons.org/licenses/by/4.0/).

1. Introduction

The global energy sector is currently confronted with a complex and urgent challenge that intersects with the domains of climate change, energy efficiency, and human comfort. Figure 1 depicts the global temperature anomalies from 1880 to 2023, with a comparative analysis to the 1951–1980 average [1]. The data demonstrate a notable increase in global temperatures, with the past nine years exhibiting the highest recorded levels. In particular, the temperature anomaly in 2023 reached 1.17 °C above the average reference period, indicating an accelerated increase in global temperatures, particularly after the 1980s. This upward trajectory reflects a growing divergence from the historical norm, with temperatures consistently rising over the past few decades. As a consequence of the warming climate, there is an anticipated surge in the demand for cooling, which will result in a significant increase in the number of air conditioning units in use worldwide. Higher ambient temperatures are directly associated with an increased use of air conditioning systems to maintain comfortable indoor environments, which will contribute to rising energy consumption. This trend suggests that without the implementation of effective mitigation strategies, there will be a compounding effect of increased greenhouse gas (GHG) emissions due to the additional energy required for cooling, which will further exacerbate the climate crisis.

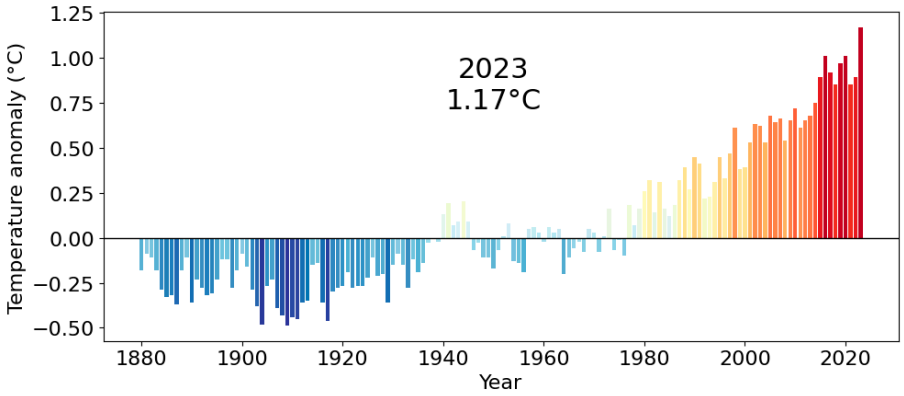


Figure 1. Global temperature anomalies (°C compared to the 1951–1980 average).

As the global population continues to grow and urbanization accelerates, the demand for cooling is dramatically increasing, particularly in developing countries with high-temperature climates [2,3]. The International Energy Agency (IEA) projects that the global demand for space cooling will triple by 2050. This surge in cooling needs coincides with an urgent imperative to curtail greenhouse gas emissions. The prevailing cooling systems, which dominate the market, present a dual challenge in this context. Firstly, these systems rely heavily on hydrofluorocarbon (HFC) refrigerants, which have global warming potentials (GWP) that are hundreds to thousands of times greater than that of CO_2 [4]. It is anticipated that global emissions of fluorinated greenhouse gases (F-gases) will increase fivefold between 2005 and 2050 (from 0.7 $PgCO_2$ eq. in 2005 to 3.7 $PgCO_2$ eq. in 2050) [5]. Secondly, these systems are substantial consumers of electricity, with a tendency to account for upward of fifty percent of peak electricity demand in climates characterized by higher temperatures [6]. Such electricity consumption not only places additional strain on power grids but also indirectly contributes to greenhouse gas emissions in regions where fossil fuels remain a significant component of the energy mix [7,8]. Moreover, the efficiency of these conventional systems tends to decline as ambient temperatures increase, creating a vicious cycle where elevated temperatures lead to augmented energy consumption for cooling, which in turn contributes to further warming [9]. This multifaceted challenge necessitates the development of innovative cooling solutions that can simultaneously address energy efficiency, environmental sustainability, and performance in a warming climate.

In the response to these challenges, integration of the organic Rankine cycle (ORC) and the vapor compression cycle (VCC) offers a promising advancement in the field of energy conversion and refrigeration technology. The ORC is renowned for its ability to recover and convert low-grade waste heat into useful work [10–12], while the VCC is widely used in refrigeration and air conditioning systems [13–15]. The integrated ORC-VCC system capitalizes on the strengths of both cycles, enhancing energy efficiency and enabling substantial waste heat recovery [16]. This pioneering system is especially commendable in that it unites the turbine and compressor stages on a single shaft, obviating the necessity for supplementary mechanical and electrical components such as couplings and generators. Consequently, the system is optimized and simplified, which may result in reduced operational and maintenance costs. Over the past decade, a substantial body of research has been conducted on the analysis of different ORC-VCC systems [17–19]. Numerous studies have explored various aspects of ORC-VCC systems, including thermodynamic modeling [20], economic feasibility [21], and the selection of working fluids [22]. These endeavors are driven by the need to improve efficiency and optimize waste heat utilization, particularly in small-scale applications where energy recovery can result in considerable cost savings and environmental benefits [22,23]. Recent experimental studies have provided significant insights into the performance of ORC-VCC systems. In article [24], the authors focused on the off-design performance of an ORC-VCC system using the low-GWP refrigerant R1234ze(E). Their experiments demonstrated that the system's coefficient of performance (COP) improved from 0.558 at a condenser heat rejection temperature of 30 °C to 0.682

at 16.6 °C. Additionally, it was observed that higher driving heat source temperatures enhanced the COP of the ORC, though this also led to a decrease in compressor efficiency. Another important experimental validation [25] highlighted that the integration of ORC and VCC in a 264 kWth system achieved a baseline COP of 0.56 with a condenser heat rejection temperature at 30 °C. The next-generation low-GWP working fluid R1234ze(E) was used. The study also noted that system performance can be significantly affected by variations in external conditions such as condenser and evaporator temperatures, which are critical for real-world applications. Similarly, in work [26], the authors conducted experiments on a thermo-mechanical refrigeration system utilizing ultra-low-temperature waste heat. Their results showed that system efficiency improved at higher heat source temperatures, with optimal performance achieved at specific conditions. The study emphasized the importance of selecting appropriate operating parameters to enhance the efficiency of ORC-VCC systems in practical applications. One of the critical factors influencing the performance of ORC-VCC systems is the choice of refrigerants. Traditional refrigerants, while effective, often have high GWP, posing environmental risks; consequently, there is a growing interest in adopting low-GWP refrigerants to reduce the environmental impact of these systems. This shift is essential for aligning energy recovery and cooling technologies with global sustainability goals [27].

The transition toward low-GWP refrigerants, driven by scientific evidence, regulatory measures, and market demand, signals the advent of a fourth generation of refrigerants with the objective of reducing their environmental impact [28,29]. Since approximately 2010, refrigerants with a GWP below 150 have been given priority, in addition to requirements for safety, compatibility, and efficiency. It is crucial to maintain high efficiency to ensure that any potential gains in GWP reduction are not offset by increased greenhouse gas emissions when efficiency is reduced. The objective of this research is to perform a multi-objective optimization of a small-scale ORC-VCC system, with a specific focus on integrating low-GWP refrigerants. A key advancement in this study is the introduction of greater flexibility in the system design. In previous studies [30], the pressure at the turbine outlet was restricted to match the compressor inlet pressure; however, this constraint has been removed, allowing for the independent optimization of these pressures. This change is crucial for improving the system's overall performance as it enables more precise tuning for efficiency and cost-effectiveness. Moreover, this study adopts a more realistic assumption for the condenser inlet temperature, setting it at 25 °C. This adjustment better represents the conditions expected in a warming climate and in cooling applications. By considering a higher inlet temperature, the model more accurately reflects the operational challenges posed by climate change, leading to a more effective and comprehensive optimization process. These enhancements—the decoupling of pressure constraints and the updated temperature assumption—are essential for optimizing the system's performance in contemporary cooling scenarios. Furthermore, there is a notable absence in the extant literature regarding the optimization of ORC-VCC system parameters, particularly with regard to the exploration of multiple degrees of freedom and the testing of various objective functions. The majority of studies have concentrated on a limited number of parameters, frequently neglecting the intricate interactions between the various components of the system. This research addresses these shortcomings by employing a comprehensive multi-objective optimization approach [31,32], incorporating multiple degrees of freedom and evaluating a range of objective functions. This study examines the potential advantages of utilizing both single- and dual-fluid configurations within the ORC-VCC system. In the single-fluid approach, the same working fluid is employed in both the ORC and VCC stages, which streamlines the system but may constrain optimization potential due to uniform thermodynamic properties. In contrast, the dual-fluid approach involves the use of distinct fluids in the ORC and VCC cycles, enabling the selection of optimal thermophysical properties tailored to each stage.

2. ORC-VCC Model Optimization Methodology

2.1. System Description and Parameters

The schematic of the thermodynamic cycle of the ORC-VCC system is depicted in Figure 2 and the T-s diagram in Figure 3. The system consists of an ORC with a regenerator subsystem and a VCC subsystem. In the course of the analyses, the potential benefits of employing both single- and dual-working-fluid approaches were explored. The former was to be utilized in an organic Rankine cycle (ORC), while the latter was to be employed in a vapor cycle combustion (VCC) system. The assumptions related to the system are detailed in Table 1. The efficiencies of the machines were selected with a significant safety margin. The internal efficiencies of both the compressor and turbine were conservatively set at 80%. The assumed values are lower than those typically reported in the recent literature for similar low-power turbomachinery.

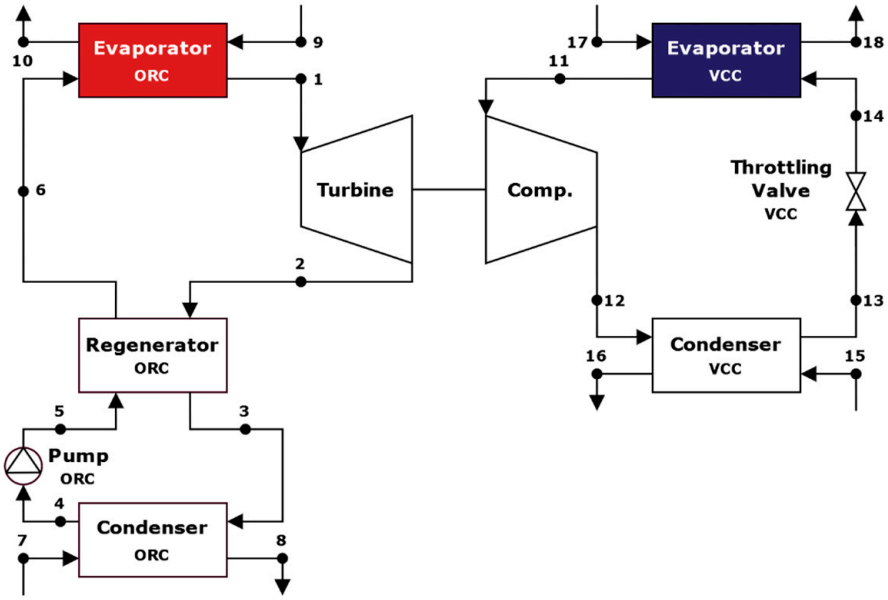


Figure 2. Schematic diagram of the ORC-VCC without electricity generation [30].

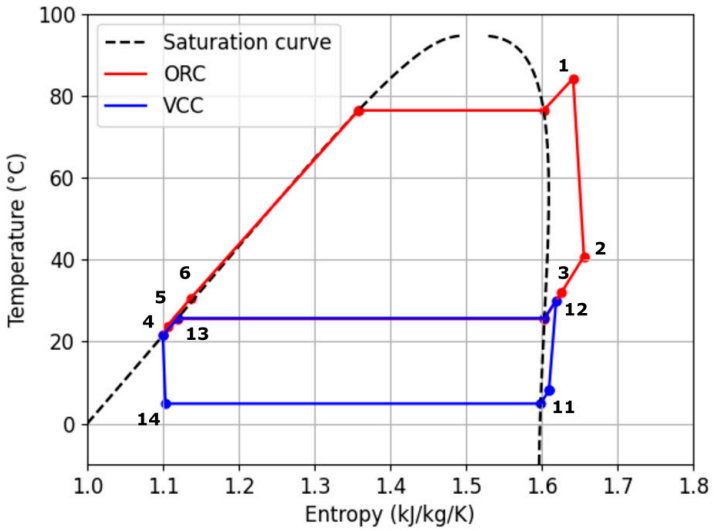


Figure 3. T-s diagram of the ORC-VCC.

Table 1. Efficiency and thermodynamic assumptions of the ORC-VCC system.

Parameter	Symbol	Unit	Value
Chilled water temperature (cold side)	T_{18}	°C	8
Chilled water temperature (hot side)	T_{17}	°C	12
Cooling water temperature (cold side)	T_7, T_{15}	°C	25
Heat source mass flow	m_9	kg/s	1
Heat source temperature (hot side)	T_9	°C	90
Compressor efficiency (VCC)	η_c	-	80% [33,34]
Pump efficiency (ORC)	η_p	-	50% [35]
Turbine efficiency (ORC)	η_t	-	80% [36,37]

2.2. Optimization Procedure and Algorithm

The optimization methodology for this study integrates advanced multi-objective optimization techniques using the pymoo library [38], a versatile Python 3.10.2 framework for multi-objective optimization, alongside a custom-developed code to accurately model and evaluate the performance of a small-scale ORC-VCC system. This combined approach enables the precise and efficient exploration of the solution space, addressing the complexity of the system's design parameters and objectives.

The ORC-VCC system is modeled using a custom code developed specifically for this study. This code simulates the thermodynamic behavior of the system, allowing for the evaluation of key performance indicators. The problem is formulated with 13 decision variables that directly influence the system's behavior, each bounded within specified limits (lower bounds of 0.1 to 50 and upper bounds of 10 to 85). The decision variables and their boundaries are showed in Table 2. These variables capture the essential parameters that affect the system's overall performance.

Table 2. Decision variables and their boundaries for the ORC-VCC system optimization.

Arg.	Parameter	Symbol	Unit	Lower Bounds	Upper Bounds
x_1	Evaporator pinch temperature difference (VCC)	ΔT_{vcc_ev}	K	3	10
x_2	Degree of superheating in evaporator (VCC)	ΔT_{vcc_sup}	K	3	10
x_3	Degree of subcooling in condenser (VCC)	ΔT_{vcc_sub}	K	3	10
x_4	Regenerator pinch temperature difference (ORC)	ΔT_{orc_reg}	K	3	15
x_5	Degree of superheating in evaporator (ORC)	ΔT_{orc_sup}	K	3	15
x_6	Degree of subcooling in condenser (ORC)	ΔT_{orc_sub}	K	7	15
x_7	Evaporator pinch temperature difference (ORC)	ΔT_{orc_ev}	K	3	10
x_8	Condenser pinch temperature difference (ORC)	ΔT_{orc_con}	K	3	10
x_9	Saturation temperature in evaporator (ORC)	T_{1sv}	°C	50	85
x_{10}	Saturation temperature in condenser (ORC)	T_{4sv}	°C	25	55
x_{11}	Chilled water mass flow rate (VCC)	m_{16}	kg/s	0.1	5
x_{12}	Pressure on the inlet of the compressor (VCC)	p_{12}	bar	0.1	10
x_{13}	Condenser pinch temperature difference (VCC)	ΔT_{vcc_con}	K	3	10

The optimization process targets three primary objectives:

- Objective Function 1: maximizing the coefficient of performance (COP), a critical measure of the system's efficiency in converting energy input into cooling output;

$$f_1 = COP = \frac{Q_{vcc_evaporator}}{Q_{orc_evaporator}} \quad (1)$$

- Objective Function 2: maximizing the cooling power, ensuring that the system can deliver the highest possible cooling capacity;

$$f_2 = Q_{vcc_evaporator} \quad (2)$$

- Objective Function 3: minimizing the pressure ratio in the compressor, which is crucial for reducing mechanical strain, size, and enhancing the system's reliability, cost savings, and longevity.

$$f_3 = \frac{p_{12}}{p_{11}} \tag{3}$$

The optimization tasks are executed using the pymoo library, which is specifically chosen for its powerful capabilities in handling multi-objective optimization problems. Pymoo supports a range of evolutionary algorithms, including the Non-dominated Sorting Genetic Algorithm III (NSGA-III) [39,40] used in this study. The NSGA-III algorithm is an effective method for solving many-objective optimization problems, comprising a series of interconnected steps. The algorithm commences with the generation of a randomly populated initial set of solutions, within defined variable bounds, and the creation of a set of pre-defined reference points in the objective space, which serve to guide the search process in a uniform manner. Subsequently, the algorithm performs non-dominated sorting, categorizing solutions into levels or "fronts" based on Pareto dominance. The initial front represents the optimal trade-offs among objectives. Each solution is associated with its nearest reference point by calculating the perpendicular distance in the objective space, thereby maintaining diversity by ensuring that solutions are distributed across different regions. The next generation is formed through environmental selection, whereby solutions are selected from the sorted fronts. In the event that the population size is exceeded, solutions that are closer to underrepresented reference points are given preference in order to prevent premature convergence. Genetic operators, such as crossover and mutation, are employed to introduce variability and explore new areas within the search space. The algorithm then iterates these steps, namely sorting, association, selection, and variation, until a termination condition is met. This may be, for example, the attainment of a pre-defined maximum number of generations or the satisfaction of a convergence criterion. Through this systematic approach, NSGA-III is able to effectively discover a diverse set of optimal solutions, thoroughly exploring the trade-offs between objectives in complex optimization tasks [41,42]. The optimization algorithm has been successfully applied in various engineering fields [43–45], including combustion chamber geometry optimization [46], the optimization of proton exchange membrane fuel cell (PEMFC)-ORC combined heat and power systems [47], and the optimization aimed at reducing emissions and fuel consumption in high-pressure common-rail diesel engines [48]. These diverse applications demonstrate the algorithm's versatility and effectiveness in addressing complex, multi-objective engineering challenges.

The optimization process is initialized by defining the problem through the class, where the custom code for ORC-VCC system calculations is embedded within the evaluation function. This function is called during each iteration of the optimization to assess the performance of each candidate solution according to the three objectives. This study systematically examines nine cases, each defined by a different combination of low-GWP refrigerants:

- a_1: R1233zd (ORC and VCC);
- a_2: R1244yd (ORC and VCC);
- a_3: R1336mzz (ORC and VCC);
- a_4: R1233zd (ORC), R1244yd (VCC);
- a_5: R1233zd (ORC), R1336mzz (VCC);
- a_6: R1244yd (ORC), R1233zd (VCC);
- a_7: R1244yd (ORC), R1336mzz (VCC);
- a_8: R1336mzz (ORC), R1233zd (VCC);
- a_9: R1336mzz (ORC), R1244yd (VCC).

These cases are designed to explore the performance impacts of different refrigerant combinations on the system's objectives. Each case is optimized separately, providing a comprehensive comparison across different fluid pairings.

For each case, the NSGA-III algorithm within pymoo is configured with a population size of 100. The algorithm uses reference directions generated by the Das–Dennis method, ensuring a well-distributed search across the three-dimensional objective space. The optimization runs for 100 generations, during which the population is refined to converge on a set of non-dominated solutions that offer the best trade-offs between maximizing the COP, maximizing cooling power, and minimizing the compressor's pressure ratio.

The combination of the pymoo library with custom ORC-VCC system modeling provides a powerful and flexible framework for this study. Pymoo's capabilities in handling multi-objective problems make it an ideal choice, particularly given the complex, non-linear relationships between the decision variables and the objectives. The custom code ensures that the thermodynamic and operational characteristics of the ORC-VCC system are accurately captured, allowing for precise evaluations of each candidate solution.

This integrated approach allows for a thorough exploration of the design space, leading to the identification of refrigerant combinations and system configurations that optimize the critical objectives. The findings are expected to provide valuable insights for the design and operational strategies of ORC-VCC systems in energy recovery and cooling applications.

3. Results and Discussion

The multi-objective optimization process yielded 90,000 outputs across nine independent optimization runs, with 13 decision variables and an objective function comprising three components. Following data cleansing, 48,642 results were deemed suitable for further analysis, with 29 key variables retained for detailed examination. These optimization runs explored various system configurations and parameter settings, yielding valuable insights into the system's behavior and performance under diverse conditions. This process facilitated the identification of optimal solutions for the ORC-VCC system.

Figure 4 shows the distribution of the 13 decision variables (x_1 to x_{13}) obtained from the optimization of the ORC-VCC system. This system was modeled using a custom-developed code specifically designed to simulate thermodynamic behavior and evaluate key performance indicators. The optimization process was performed using NSGA-III, which is well-suited for multi-objective optimization tasks and allows for effective exploration of the decision space to find a set of optimal solutions across competing objectives. Each decision variable plays a critical role in influencing the system's behavior, and its ranges are constrained by specified lower and upper bounds of the optimization process. The box plot shows the distribution of each decision variable after standardization, providing a clear representation of its behavior relative to the optimization bounds. The boxes represent the interquartile range (IQR) for each variable, encapsulating the middle 50% of the data, while the central line within each box marks the median, providing insight into the central tendency of the variables. The whiskers indicate the variability outside the IQR and individual points beyond the whiskers are considered outliers, highlighting the occurrence of extreme values. The optimization bounds are indicated by different markers: the lower bounds are represented by white squares with black outlines, while the upper bounds are marked by white triangles with black outlines. These markers illustrate the limits within which each variable was allowed to vary during the optimization process. For several variables, such as x_1 through x_4, the bounds are positioned close to the observed distribution, indicating that these decision variables were tightly controlled, whereas for variables such as x_9 and x_{10}, the upper bounds are positioned significantly away from the median, indicating that greater flexibility was allowed during the optimization. This indicates that these variables had a wider feasible space to explore in the search for optimal configurations. The presence of a significant number of outliers for variables such as x_5, x_9, x_{10}, and x_{12} reflects the presence of extreme values identified during the optimization, possibly corresponding to specific scenarios where these configurations offered distinct performance advantages. In contrast, other variables, such as x_1, x_2, and x_3, exhibit less variability and fewer outliers, suggesting that the optimal values for these variables were more consistently located within a narrow range.

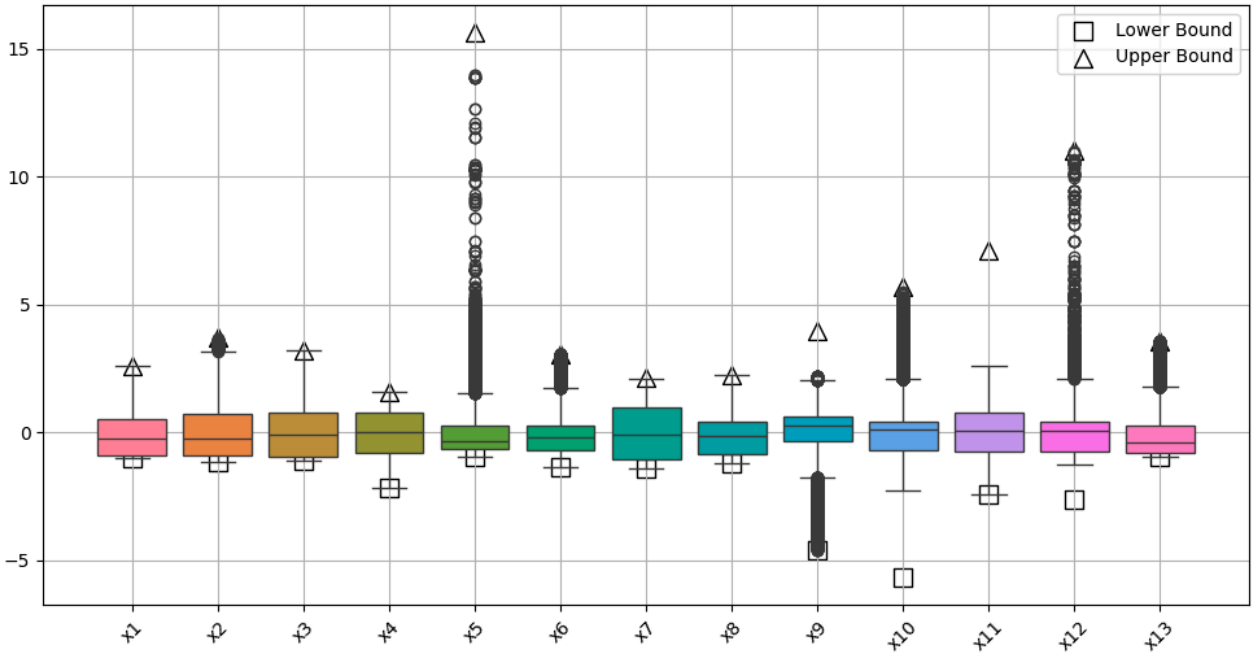


Figure 4. The distribution of decision variables in the optimization runs.

A consistent trend is observed in Figures 5–13, whereby the highest (COP) values are achieved at the lowest feasible compressor pressure ratios. This observation reflects the inverse relationship between temperature lift and the COP in refrigeration systems. The temperature lift, defined as the difference between the condenser and evaporator temperatures, is primarily determined by the operating pressures of the VCC system. Lower compressor pressure ratios result in a smaller temperature lift, which means the compressor requires less work to transfer heat from the evaporator to the condenser. Consequently, the system operates more efficiently, leading to higher COP values. Figures 5–7 illustrate the relationship between the coefficient of performance, the pressure ratio, and the cooling capacity for different refrigerants in an ORC-VCC configuration, specifically for R1233zd, R1244yd, and R1336mzz. All figures show a similar trend, where higher COP values are predominantly found at lower pressure ratios, which also corresponds to a relatively high cooling capacity range. For R1233zd (Figure 5), the COP peaks at around 0.5 when the pressure ratio is between 3 and 6, and the corresponding cooling capacity reaches up to 30 kW. Similarly, for R1244yd (Figure 6), the maximum COP is around 0.4, occurring at pressure ratios between 3 and 5, with a cooling capacity of around 30 kW. The trend for R1336mzz (Figure 7) follows a similar pattern, with a maximum COP of about 0.5 achieved at pressure ratios between 4 and 6, while the cooling capacity reaches up to 35 kW. All three fluids show a decrease in the COP as the pressure ratio increases beyond 6, suggesting that the performance of these systems is optimal at moderate pressure ratios. It is evident that although each working fluid exhibits different behavior, the cooling capacity and COP decrease at higher pressure ratios, indicating a trade-off between system efficiency and working fluid selection. In addition, the distribution of data points shows that R1336mzz has a wider operating range with the highest cooling capacity recorded among the three fluids. This suggests that R1336mzz may be more suitable for applications requiring higher cooling capacities, while R1233zd and R1244yd may be advantageous in scenarios where efficiency is prioritized at lower pressure ratios.

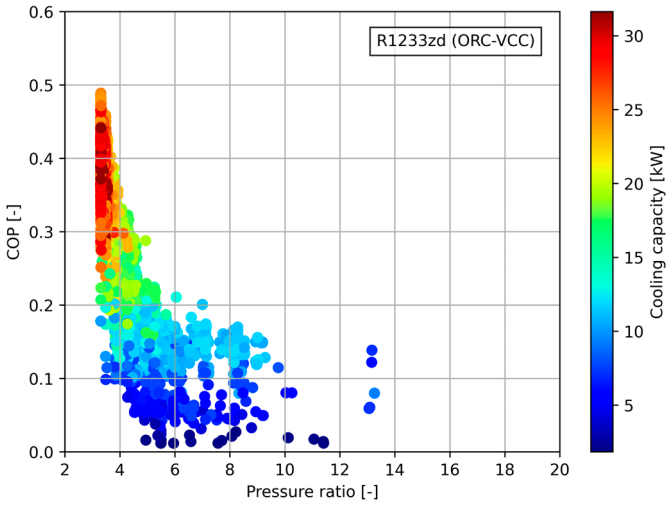


Figure 5. Relationship between COP, pressure ratio, and cooling generation for R1233zd.

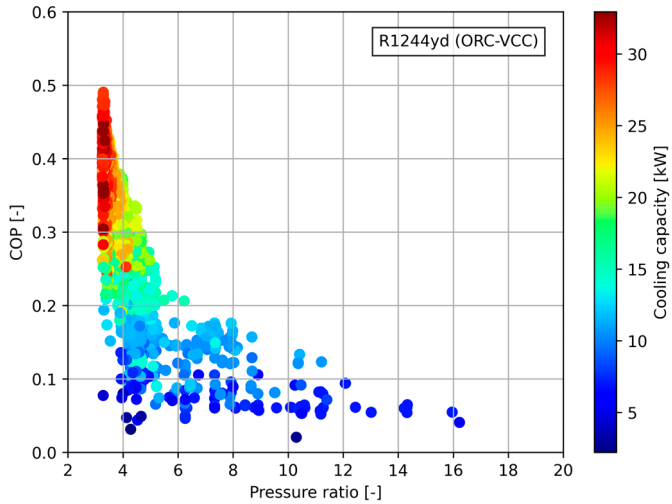


Figure 6. Relationship between COP, pressure ratio, and cooling generation for R1244yd.

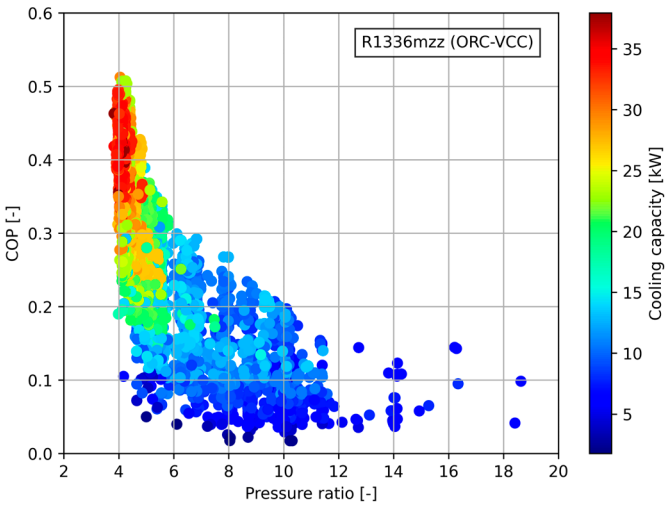


Figure 7. Relationship between COP, pressure ratio, and cooling generation for R1336mzz.

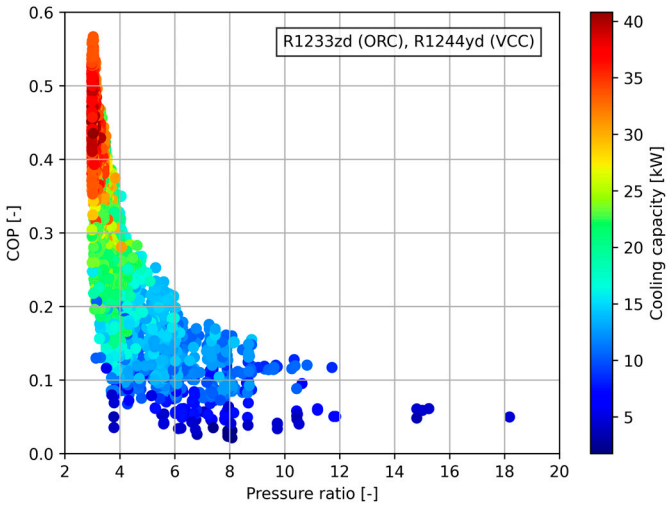


Figure 8. Relationship between COP, pressure ratio, and cooling generation for R1233zd in ORC cycle and R1244yd in VCC cycle.

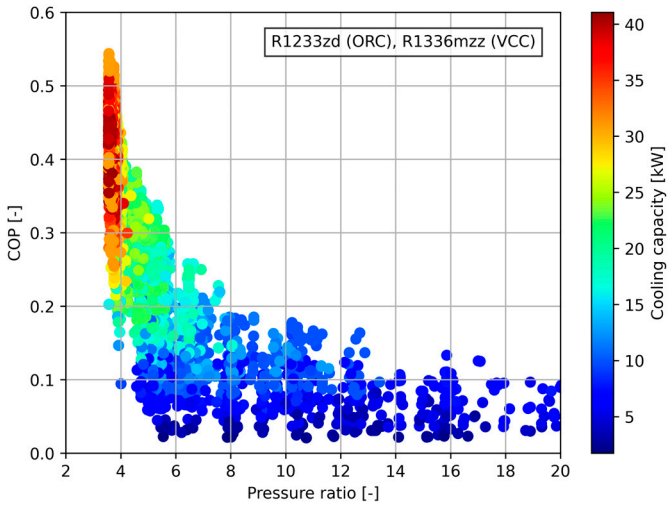


Figure 9. Relationship between COP, pressure ratio, and cooling generation for R1233zd in ORC cycle and R1336mzz in VCC cycle.

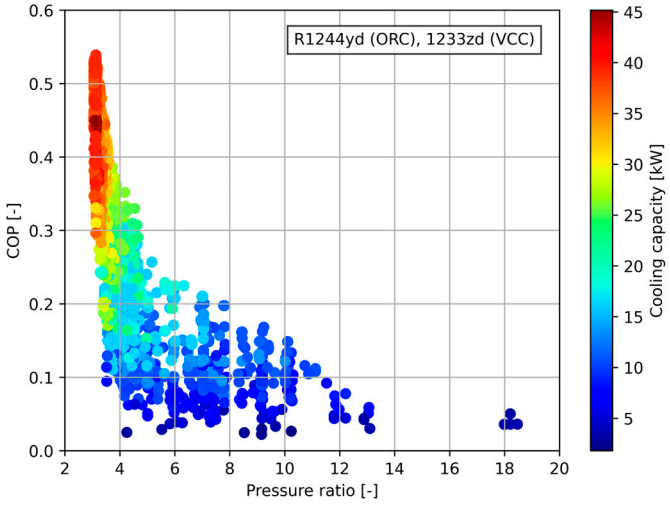


Figure 10. Relationship between COP, pressure ratio, and cooling generation for R1244yd in ORC cycle and R1233zd in VCC cycle.

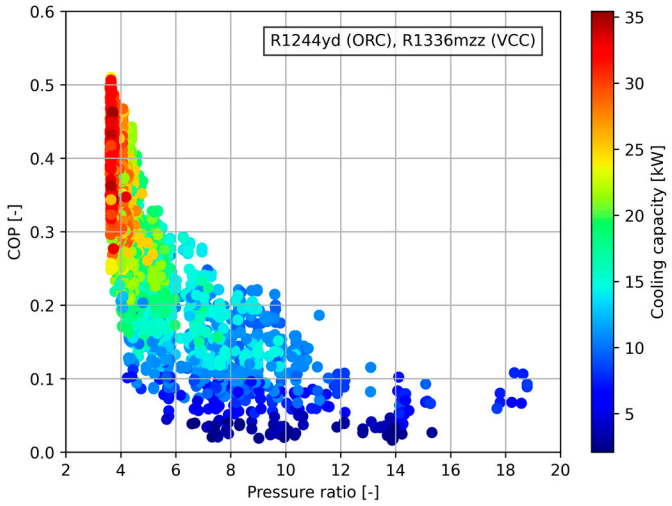


Figure 11. Relationship between COP, pressure ratio, and cooling generation for R1244yd in ORC cycle and R1336mzz in VCC cycle.

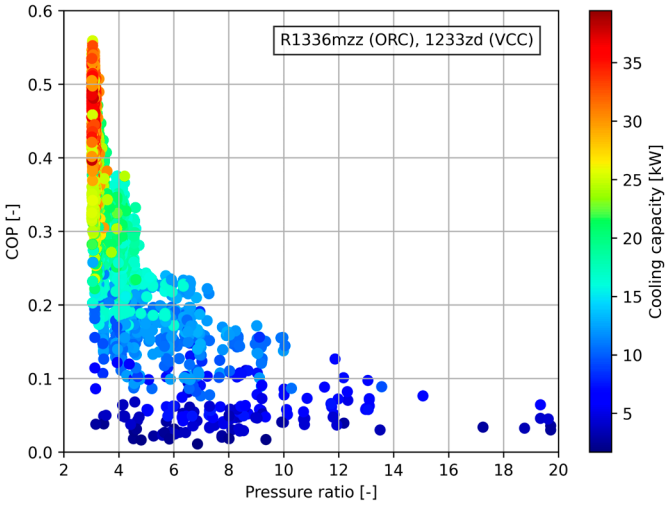


Figure 12. Relationship between COP, pressure ratio, and cooling generation for R1336mzz in ORC cycle and R133zd in VCC cycle.

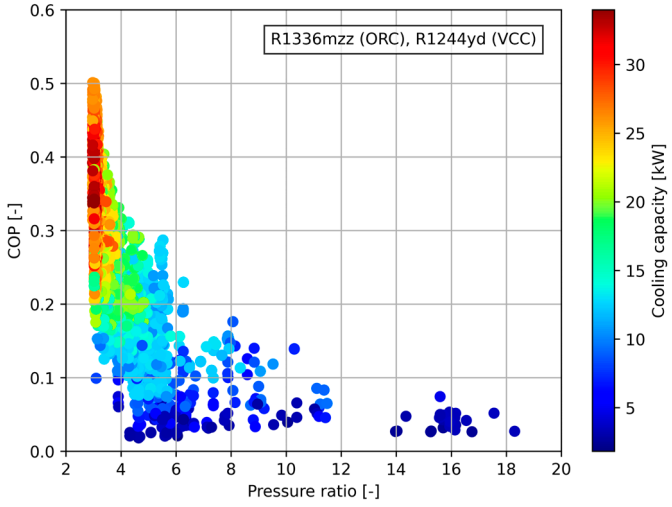


Figure 13. Relationship between COP, pressure ratio, and cooling generation for R1336mzz in ORC cycle and R1224yd in VCC cycle.

Figures 8–13 demonstrate the relationship between the COP, pressure ratio, and cooling capacity for a dual-fluid approach using different fluids in the ORC-VCC. The analysis explores the impact of combining different fluids—one in the ORC cycle and the other in the VCC cycle—to optimize system performance for power and refrigeration generation. Figure 8 represents the combination of R1233zd in the ORC cycle and R1244yd in the VCC cycle. The maximum COP achieved is around 0.57 at a pressure ratio between 3 and 4, while the cooling capacity reaches up to 41 kW. This combination shows optimal performance at lower pressure ratios, with both COP and cooling capacity decreasing significantly beyond a pressure ratio of 6.

Figure 9 examines the use of R1233zd in the ORC and R1336mzz in the VCC cycle. The COP peaks at approximately 0.54, again at low pressure ratios (around 3.8–4). The maximum cooling capacity for this configuration is also around 41 kW. Compared to the combination in Figure 9, the operational range is slightly broader but the trends in terms of efficiency and cooling capacity are consistent.

Figure 10 shows the performance of R1244yd in the ORC cycle combined with R1233zd in the VCC cycle. This pairing shows the highest cooling capacity of the combinations analyzed, reaching up to 45.16 kW with a peak COP of 0.54 at pressure ratios between 3 and 3.8. This combination could be advantageous for applications where maximizing cooling capacity is critical.

Figure 11 illustrates the combination of R1244yd in the ORC cycle and R1336mzz in the VCC cycle. The peak COP for this configuration is about 0.51 at pressure ratios between 3.5 and 4 and the cooling capacity reaches a maximum of about 35.44 kW. Efficiency decreases above a pressure ratio of 8, indicating that this pair, like the other combinations, works best at moderate pressure ratios.

Figure 12 explores the use of R1336mzz in the ORC cycle and R1233zd in the VCC cycle. The maximum COP achieved is around 0.56 at low pressure ratios (3–3.5), while the cooling capacity is around 39.45 kW. This combination, while still efficient at lower pressure ratios, shows a lower overall performance in terms of cooling capacity compared to other combinations, indicating that it may be less suitable for high-power cooling applications.

Figure 13 shows the performance of the combination of R1336mzz in the ORC cycle and R1244yd in the VCC cycle. The maximum COP is approximately 0.50, with a cooling capacity of up to 34 kW. This is the lowest cooling capacity observed among the combinations analyzed, suggesting that this pair may be more appropriate in scenarios where efficiency is prioritized over cooling capacity.

Table 3 irrefutably demonstrates that the dual-fluid approach outperforms the single-fluid approach in all key parameters, including the pressure ratio, COP, and cooling capacity. This distinction is particularly evident when comparing cases a_1–a_3, which employ a single-fluid approach, with cases a_4–a_9, which utilize a dual-fluid approach. The minimum pressure ratio observed for the dual-fluid approach (cases a_4–a_9) is 2.97, as seen in case a_9. In contrast, the minimum pressure ratio for the single-fluid approach (cases a_1–a_3) is 3.25, as observed in case a_2. A lower pressure ratio is indicative of a more straightforward turbocompressor configuration. Lower pressure ratios can reduce the design complexity, minimize material stress, and potentially lower manufacturing and operational costs. In dual-fluid cases, the maximum COP is 0.57, which is achieved in case a_4. In comparison, the maximum COP for the single-fluid approach is 0.51, as observed in case a_3. The higher coefficient of performance observed in the dual-fluid configuration indicates an overall improvement in system energy efficiency, suggesting that the dual-fluid approach is more effective in converting energy inputs into useful cooling. The maximum cooling capacity for the dual-fluid approach is markedly greater than that of the single-fluid approach, at 45.16 kW (case a_6) compared to 37.94 kW (case a_3). This indicates that the dual-fluid configuration is capable of delivering a significantly higher cooling output, rendering it a more suitable option for applications requiring high cooling loads. The ORC turbine power output ranges from 4.93 kW to 6.73 kW, indicating varying levels of energy recovery across different conditions. This power generation is solely dedicated to covering the energy

consumption of the compressor. In contrast, the ORC feed pump power consumption varies between 0.12 kW and 0.25 kW, demonstrating a relatively low energy demand in comparison to the turbine output. The efficiency of the ORC system exhibits a range of 5.97% to 8.52%, demonstrating a lack of proportional growth in tandem with the system's COP.

Table 3. Comparison of best results for specific cases.

Parameter	Pressure Ratio [-]	COP [-]	Cooling Capacity [kW]	ORC Turbine [kW]	ORC Feed Pump [kW]	ORC Efficiency [%]	Case
Minimum pressure ratio (all cases)	2.97	0.41	32.93	4.93	0.12	5.97	a_9
Maximum COP (all cases)	3.03	0.57	33.67	5.02	0.18	8.16	a_4
Maximum cooling capacity (all cases)	3.10	0.45	45.16	6.73	0.25	6.43	a_6
Minimum pressure ratio (1–3 cases)	3.25	0.42	29.56	5.10	0.20	6.98	a_2
Maximum COP (1–3 cases)	4.05	0.51	29.51	5.03	0.13	8.52	a_3
Maximum cooling capacity (1–3 cases)	4.12	0.44	37.94	6.52	0.15	7.49	a_3

In a related finding [49], the ORC-FTVIC-D (Flash Tank Vapor Injection Cycle) system, operating with a heat source temperature of 100 °C (90 °C in the present analysis), yielded a COP below 0.3 with the working fluids R1270 (ORC) and R152a (VCC). An increase in the heat source temperature to 150 °C resulted in a notable improvement in the COP, reaching a value of up to 0.55. In contrast, Grauberger et al. [25] reported a COP of 0.65 for a single-fluid system (R1234ze(E)) with a heat source temperature of 91 °C. The main differences between the presented system and those available in the literature are the configuration of the system (which includes a shared economizer) and the power output, which is tenfold higher in the referenced study.

Pareto frontiers for both single-fluid and dual-fluid approaches, focusing on the relationships between the COP, cooling capacity, and pressure ratio, are shown in Figures 14–16. These figures are critical for identifying optimal trade-offs between system efficiency (COP) and performance metrics such as cooling capacity and pressure ratio.

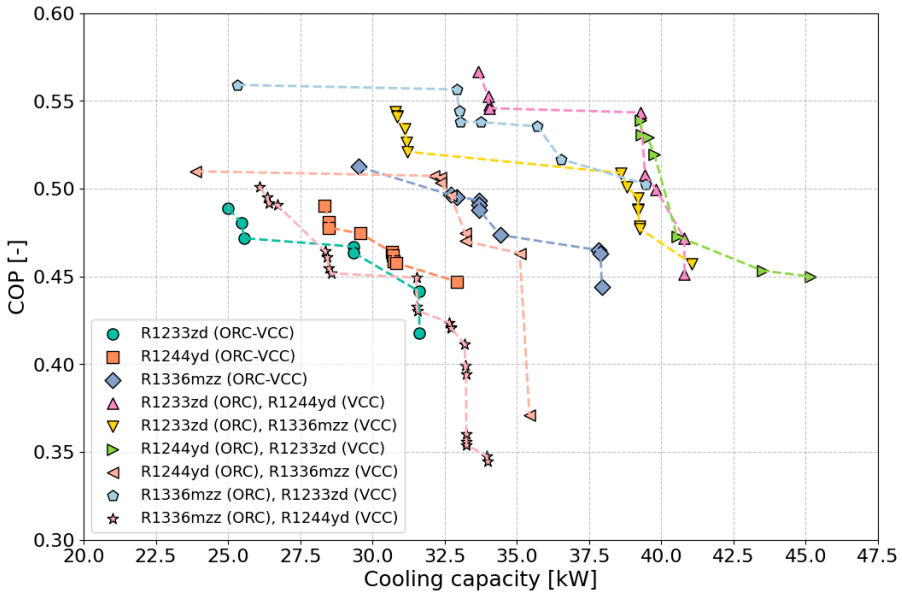


Figure 14. Pareto frontier for single- and dual-fluid approaches (COP vs. cooling capacity).

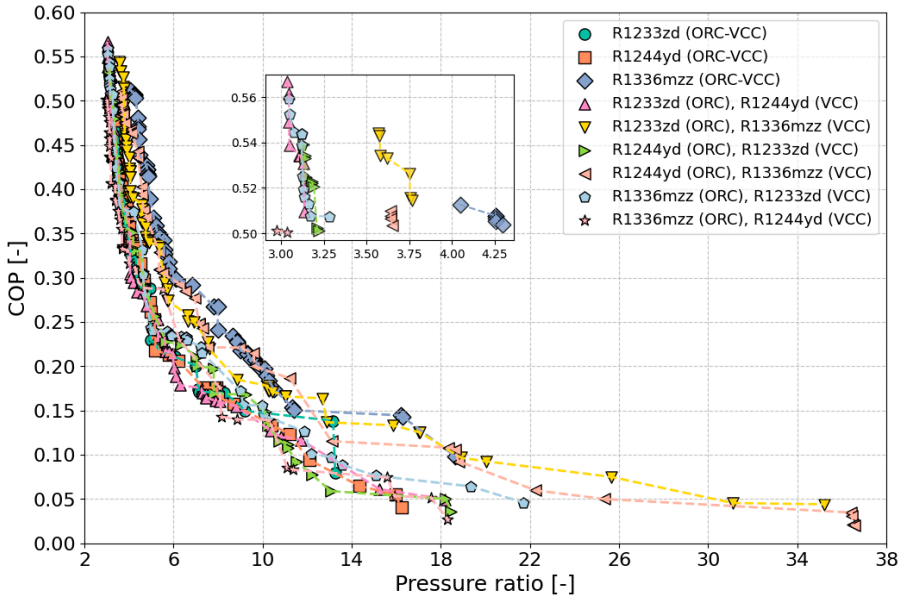


Figure 15. Pareto frontier for single- and dual-fluid approaches (COP vs. pressure ratio).

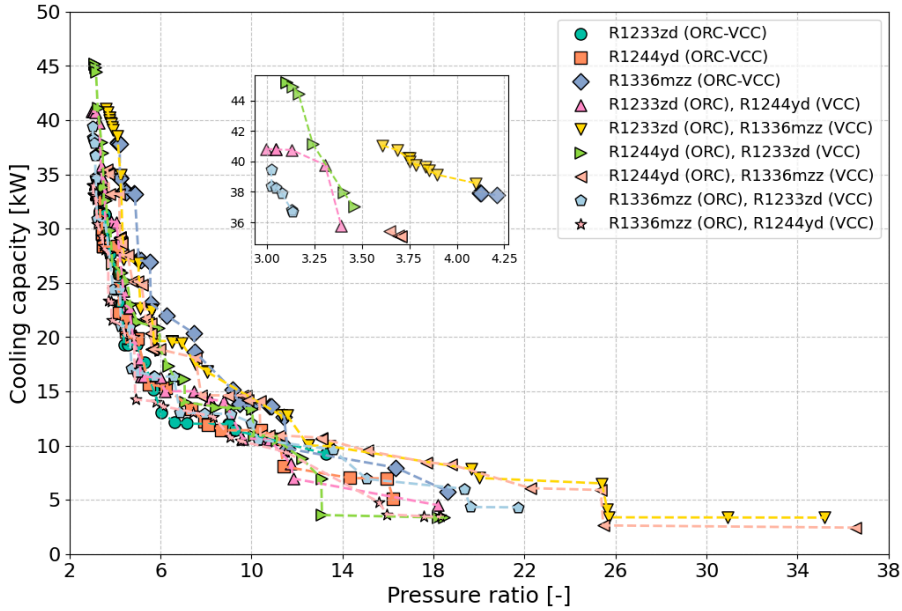


Figure 16. Pareto frontier for single- and dual-fluid approaches (cooling capacity vs. pressure ratio).

Figure 14 compares the COP versus cooling capacity for single-fluid and dual-fluid configurations. Dual-fluid combinations—particularly R1244yd (ORC) with R1233zd (VCC)—achieve significantly higher cooling capacities, up to 45 kW, while maintaining COP values in the 0.45–0.5 range. Conversely, single-fluid systems exhibit comparatively lower cooling capacities, indicating a performance limitation compared to their dual-fluid counterparts. Figure 15 shows the COP versus pressure ratio for both approaches. Higher COP values are consistently observed at lower pressure ratios (<10) for all configurations. Dual-fluid systems show superior performance over a wider operating range, with higher efficiencies at moderate pressure ratios compared to single-fluid systems, which show a more rapid decline in the COP with increasing pressure. The relationship between the cooling capacity and the pressure ratio is shown in Figure 16. Dual-fluid configurations exhibit the highest cooling capacities at moderate pressure ratios (<10), while single-fluid systems fall short in maximizing cooling capacity. This underscores the superior ability of dual-fluid systems to optimize cold generation at efficient pressure conditions. The trends displayed in both

Figures 15 and 16 exhibit comparable patterns, which can be attributed to the intrinsic relationship between the COP and cooling capacity. The nature of these trends is associated with the algorithm's objective of minimizing the compressor outlet temperature, which in turn allows for a lower inlet temperature to the VCC evaporator. The specified computational assumptions, including chilled water temperatures and a lower evaporator inlet temperature, among others, enable the system to achieve higher cooling capacity values.

The adoption of low-GWP refrigerants presents a significant opportunity to reduce GHG emissions. As an illustration, the replacement of R245fa (GWP 1030) with analyzed R1233zd (GWP 1) in air conditioning systems has the potential to reduce refrigerant-related GHG emissions by approximately 99%. With an average charge of 10 kg per unit and a 2% annual leakage rate taken into account, the resulting annual emission reduction per unit is presented below.

$$\text{Emmission reduction} = \left(\text{GWP}_{\text{high}} - \text{GWP}_{\text{low}}\right) \times \text{released mass of fluid} \quad (4)$$

$$\text{Emmission reduction} = (1030 - 1) \times 10\ \text{kg} \times 0.02 = 205.8\ \text{CO}_2\text{eq} \quad (5)$$

The application of this approach to a city with 100,000 units results in an annual reduction of over 20.58 metric tons of CO_2 equivalent emissions.

4. Conclusions

This work demonstrates the significant advantages of using an advanced dual-fluid approach to optimize the performance of a small-scale ORC-VCC system, resulting in superior energy efficiency and improved environmental sustainability. The optimized dual-fluid configuration, specifically using R1244yd in ORC and R1233zd in VCC, achieved significant improvements in all critical parameters:

- The dual-fluid configuration achieved a high COP of 0.57, indicating high cycle efficiency. The system delivered a cooling capacity of 45.16 kW, meeting substantial cooling demands;
- The reduced pressure ratios lowered mechanical stress and operational complexity, enhancing system reliability;
- The dual-fluid setup proved to be more robust and flexible than single-fluid approaches, offering enhanced system performance and adaptability.

The multi-objective optimization was conducted in an effective manner using the NSGA-III. The implementation of this sophisticated algorithm enabled the following:

- The algorithm facilitated efficient navigation of the complex design space. The algorithm enabled the exploration of a comprehensive range of design variables and system configurations;
- The identification of optimal trade-offs was also facilitated. The system enabled a balance to be struck between three key objectives: maximizing efficiency, increasing cooling capacity, and minimizing pressure ratios;
- A comprehensive optimization process was employed. The intricate interactions between system components were successfully captured, resulting in comprehensive performance enhancements.

In addition, the dual-fluid approach offers significant advances in reducing the environmental impact of cooling technologies by minimizing the use of high-GWP refrigerants while maximizing energy recovery potential. These findings underscore the transformative potential of dual-fluid ORC-VCC systems for applications requiring both high efficiency and reduced carbon footprint, supporting the global shift toward sustainable cooling solutions. The findings presented in this work also lay the foundation for future research on integrated thermal management systems, with a focus on multi-objective optimization that bridges the gap between operational performance, environmental responsibility, and cost-effectiveness.

Funding: This research was supported by the National Centre for Research and Development (NCBR) through the LIDER XIV programme within the COOLERHEAT project (Grant Agreement Number LIDER14/0173/2023).

Data Availability Statement: The original contributions presented in this study are included in the article, further inquiries can be directed to the corresponding author.

Conflicts of Interest: The author declares no conflicts of interest.

References

1. NASA Earth Observatory. Available online: https://earthobservatory.nasa.gov/world-of-change/global-temperatures (accessed on 29 September 2024).
2. Isaac, M.; van Vuuren, D.P. Modeling Global Residential Sector Energy Demand for Heating and Air Conditioning in the Context of Climate Change. *Energy Policy* **2009**, *37*, 507–521. [CrossRef]
3. Berardi, U.; Jafarpur, P. Assessing the Impact of Climate Change on Building Heating and Cooling Energy Demand in Canada. *Renew. Sustain. Energy Rev.* **2020**, *121*, 109681. [CrossRef]
4. Velders, G.J.M.; Fahey, D.W.; Daniel, J.S.; McFarland, M.; Andersen, S.O. The Large Contribution of Projected HFC Emissions to Future Climate Forcing. *Proc. Natl. Acad. Sci. USA* **2009**, *106*, 10949–10954. [CrossRef] [PubMed]
5. Purohit, P.; Höglund-Isaksson, L. Global Emissions of Fluorinated Greenhouse Gases 2005–2050 with Abatement Potentials and Costs. *Atmos. Chem. Phys.* **2017**, *17*, 2795–2816. [CrossRef]
6. Santamouris, M. Cooling the Buildings—Past, Present and Future. *Energy Build.* **2016**, *128*, 617–638. [CrossRef]
7. Waite, M.; Cohen, E.; Torbey, H.; Piccirilli, M.; Tian, Y.; Modi, V. Global Trends in Urban Electricity Demands for Cooling and Heating. *Energy* **2017**, *127*, 786–802. [CrossRef]
8. Agarwal, S.; Rengarajan, S.; Sing, T.F.; Yang, Y. Nudges from School Children and Electricity Conservation: Evidence from the "Project Carbon Zero" Campaign in Singapore. *Energy Econ.* **2017**, *61*, 29–41. [CrossRef]
9. Tang, F.; Gao, J.; Wu, X.; Hu, G.; Yao, H.; Zhu, X. Performance Investigation on a Precision Air Conditioning System with a Condensation Heat Recovery Unit under Varying Operating Conditions. *Appl. Therm. Eng.* **2024**, *236*, 121664. [CrossRef]
10. Almehmadi, F.A.; Elattar, H.F.; Fouda, A.; Alqaed, S.; Mustafa, J.; Alharthi, M.A.; Refaey, H.A. Energy Performance Assessment of a Novel Solar Poly-Generation System Using Various ORC Working Fluids in Residential Buildings. *Energies* **2022**, *15*, 8286. [CrossRef]
11. Almehmadi, F.A.; Elattar, H.F.; Fouda, A.; Alqaed, S.; Alharthi, M.A.; Refaey, H.A. Towards an Efficient Multi-Generation System Providing Power, Cooling, Heating, and Freshwater for Residential Buildings Operated with Solar-Driven ORC. *Appl. Sci.* **2022**, *12*, 11157. [CrossRef]
12. Kaczmarczyk, T.Z.; Żywica, G. Experimental Study of the Effect of Load and Rotational Speed on the Electrical Power of a High-Speed ORC Microturbogenerator. *Appl. Therm. Eng.* **2024**, *238*, 122012. [CrossRef]
13. Pan, M.; Zhao, H.; Liang, D.; Zhu, Y.; Liang, Y.; Bao, G. A Review of the Cascade Refrigeration System. *Energies* **2020**, *13*, 2254. [CrossRef]
14. Saeed, M.Z.; Contiero, L.; Blust, S.; Allouche, Y.; Hafner, A.; Eikevik, T.M. Ultra-Low-Temperature Refrigeration Systems: A Review and Performance Comparison of Refrigerants and Configurations. *Energies* **2023**, *16*, 7274. [CrossRef]
15. Tassou, S.A.; Lewis, J.S.; Ge, Y.T.; Hadawey, A.; Chaer, I. A Review of Emerging Technologies for Food Refrigeration Applications. *Appl. Therm. Eng.* **2010**, *30*, 263–276. [CrossRef]
16. Lecompte, S.; Huisseune, H.; Van Den Broek, M.; Vanslambrouck, B.; De Paepe, M. Review of Organic Rankine Cycle (ORC) Architectures for Waste Heat Recovery. *Renew. Sustain. Energy Rev.* **2015**, *47*, 448–461. [CrossRef]
17. Aphornratana, S.; Sriveerakul, T. Analysis of a Combined Rankine-Vapour-Compression Refrigeration Cycle. *Energy Convers. Manag.* **2010**, *51*, 2557–2564. [CrossRef]
18. Wang, H.; Peterson, R.; Herron, T. Design Study of Configurations on System COP for a Combined ORC (Organic Rankine Cycle) and VCC (Vapor Compression Cycle). *Energy* **2011**, *36*, 4809–4820. [CrossRef]
19. Toujeni, N.; Bouaziz, N.; Kairaouani, L. Energetic Investigation of a New Combined ORC-VCC System for Cogeneration. *Energy Procedia* **2017**, *139*, 670–675. [CrossRef]
20. Asim, M.; Leung, M.K.H.; Shan, Z.; Li, Y.; Leung, D.Y.C.; Ni, M. Thermodynamic and Thermo-Economic Analysis of Integrated Organic Rankine Cycle for Waste Heat Recovery from Vapor Compression Refrigeration Cycle. *Energy Procedia* **2017**, *143*, 192–198. [CrossRef]
21. Aryanfar, Y.; Assad, M.E.H.; Khosravi, A.; Atiqure, R.S.M.; Sharma, S.; Alcaraz, J.L.G.; Alayi, R. Energy, Exergy and Economic Analysis of Combined Solar ORC-VCC Power Plant. *Int. J. Low-Carbon Technol.* **2022**, *17*, 196–205. [CrossRef]
22. Nasir, M.T.; Kim, K.C. Working Fluids Selection and Parametric Optimization of an Organic Rankine Cycle Coupled Vapor Compression Cycle (ORC-VCC) for Air Conditioning Using Low Grade Heat. *Energy Build.* **2016**, *129*, 378–395. [CrossRef]
23. Karellas, S.; Braimakis, K. Energy-Exergy Analysis and Economic Investigation of a Cogeneration and Trigeneration ORC-VCC Hybrid System Utilizing Biomass Fuel and Solar Power. *Energy Convers. Manag.* **2016**, *107*, 103–113. [CrossRef]
24. Grauberger, A.; Young, D.; Bandhauer, T. Off-Design Performance of an Organic Rankine-Vapor Compression Cooling Cycle Using R1234ze(E). *Appl. Energy* **2022**, *321*, 119421. [CrossRef]

25. Grauberger, A.; Young, D.; Bandhauer, T. Experimental Validation of an Organic Rankine-Vapor Compression Cooling Cycle Using Low GWP Refrigerant R1234ze(E). *Appl. Energy* **2022**, *307*, 118242. [CrossRef]
26. Sleiti, A.K.; Al-Ammari, W.A.; Al-Khawaja, M. Experimental Investigations on the Performance of a Thermo-Mechanical Refrigeration System Utilizing Ultra-Low Temperature Waste Heat Sources. *Alex. Eng. J.* **2023**, *71*, 591–607. [CrossRef]
27. Asim, M.; Kashif, F.; Umer, J.; Alvi, J.Z.; Imran, M.; Khan, S.; Zia, A.W.; Leung, M.K.H. Performance Assessment and Working Fluid Selection for Novel Integrated Vapor Compression Cycle and Organic Rankine Cycle for Ultra Low Grade Waste Heat Recovery. *Sustainability* **2021**, *13*, 11592. [CrossRef]
28. Calm, J.M. The next Generation of Refrigerants—Historical Review, Considerations, and Outlook. *Int. J. Refrig.* **2008**, *31*, 1123–1133. [CrossRef]
29. Wang, J.; Gullo, P.; Ramezani, H. Review on the Trend of Ultra-Low-GWP Working Fluids for Small-Capacity Vapour-Compression Systems. *Sustain. Energy Technol. Assess.* **2024**, *66*, 103803. [CrossRef]
30. Witanowski, Ł. Comprehensive Analysis of ORC-VCC System for Air Conditioning from Low-Temperature Waste Heat. In Proceedings of the 7th International Seminar on ORC Power System (ORC 2023), Seville, Spain, 4–6 September 2023; Editorial Universidad de Sevilla: Seville, Spain, 2024; pp. 203–213.
31. Mesloub, A.; Hafnaoui, R.; Hassan Abdelhafez, M.H.; Seghier, T.E.; Kolsi, L.; Ben Ali, N.; Ghosh, A. Multi-Objective Optimization of Switchable Suspended Particle Device Vacuum Glazing for Comfort and Energy Efficiency in School Typologies under Hot Climate. *Case Stud. Therm. Eng.* **2024**, *61*, 105039. [CrossRef]
32. Wang, L.; Yang, J.; Qu, B.; Pang, C. Multi-Objective Optimization of an Organic Rankine Cycle (ORC) for a Hybrid Solar–Waste Energy Plant. *Energies* **2024**, *17*, 1810. [CrossRef]
33. Uusitalo, A.; Turunen-Saaresti, T.; Honkatukia, J.; Tiainen, J.; Jaatinen-Värri, A. Numerical Analysis of Working Fluids for Large Scale Centrifugal Compressor Driven Cascade Heat Pumps Upgrading Waste Heat. *Appl. Energy* **2020**, *269*, 115056. [CrossRef]
34. Wang, Y.; Lin, F.; Nie, C.; Engeda, A. Design and Performance Evaluation of a Very Low Flow Coefficient Centrifugal Compressor. *Int. J. Rotating Mach.* **2013**, *2013*, 293486. [CrossRef]
35. de Neto, R.O.; Sotomonte, C.A.R.; Coronado, C.J.R. Off-Design Model of an ORC System for Waste Heat Recovery of an Internal Combustion Engine. *Appl. Therm. Eng.* **2021**, *195*, 117188. [CrossRef]
36. Da Lio, L.; Manente, G.; Lazzaretto, A. New Efficiency Charts for the Optimum Design of Axial Flow Turbines for Organic Rankine Cycles. *Energy* **2014**, *77*, 447–459. [CrossRef]
37. Xu, G.; Zhao, G.; Quan, Y.; Liang, R.; Li, T.; Dong, B.; Fu, J. Design and Optimization of a Radial-Axial Two-Stage Coaxial Turbine for High-Temperature Supercritical Organic Rankine Cycle. *Appl. Therm. Eng.* **2023**, *227*, 120365. [CrossRef]
38. Blank, J.; Deb, K. Pymoo: Multi-Objective Optimization in Python. *IEEE Access* **2020**, *8*, 89497–89509. [CrossRef]
39. Deb, K.; Jain, H. An Evolutionary Many-Objective Optimization Algorithm Using Reference-Point-Based Nondominated Sorting Approach, Part I: Solving Problems With Box Constraints. *IEEE Trans. Evol. Comput.* **2014**, *18*, 577–601. [CrossRef]
40. Jain, H.; Deb, K. An Evolutionary Many-Objective Optimization Algorithm Using Reference-Point Based Nondominated Sorting Approach, Part II: Handling Constraints and Extending to an Adaptive Approach. *IEEE Trans. Evol. Comput.* **2014**, *18*, 602–622. [CrossRef]
41. Deb, K.; Pratap, A.; Agarwal, S.; Meyarivan, T. A Fast and Elitist Multiobjective Genetic Algorithm: NSGA-II. *IEEE Trans. Evol. Comput.* **2002**, *6*, 182–197. [CrossRef]
42. Petchrompo, S.; Coit, D.W.; Brintrup, A.; Wannakrairot, A.; Parlikad, A.K. A Review of Pareto Pruning Methods for Multi-Objective Optimization. *Comput. Ind. Eng.* **2022**, *167*, 108022. [CrossRef]
43. Aieneh, K.; Mehranfar, S.; Yazdi Sotoude, M.; Sadeghi, S.; Mahmoudzadeh Andwari, A. Solar-Powered Combined Cooling, Heating, and Power Energy System with Phase-Change Material and Water Electrolysis: Thermo-Economic Assessment and Optimization. *Energies* **2024**, *17*, 3309. [CrossRef]
44. Wang, X.; Chen, X.; Xing, C.; Ping, X.; Zhang, H.; Yang, F. Performance Analysis and Rapid Optimization of Vehicle ORC Systems Based on Numerical Simulation and Machine Learning. *Energies* **2024**, *17*, 4542. [CrossRef]
45. Aram, K.; Taherkhani, R.; Šimelytė, A. Multistage Optimization toward a Nearly Net Zero Energy Building Due to Climate Change. *Energies* **2022**, *15*, 983. [CrossRef]
46. Gao, S.; Zhang, Y.; Zhang, Z.; Tan, D.; Li, J.; Yin, Z.; Hu, J.; Zhao, Z. Multi-Objective Optimization of the Combustion Chamber Geometry for a Highland Diesel Engine Fueled with Diesel/n-Butanol/PODEn by ANN-NSGA III. *Energy* **2023**, *282*, 128793. [CrossRef]
47. Lu, X.; Du, B.; Zhu, W.; Yang, Y.; Xie, C.; Tu, Z.; Zhao, B.; Zhang, L.; Wang, J.; Yang, Z. Multi-Criteria Assessment of an Auxiliary Energy System for Desalination Plant Based on PEMFC-ORC Combined Heat and Power. *Energy* **2024**, *290*, 130163. [CrossRef]
48. Wang, Y.; Wang, G.; Yao, G.; Shen, Q.; Yu, X.; He, S. Combining GA-SVM and NSGA-III Multi-Objective Optimization to Reduce the Emission and Fuel Consumption of High-Pressure Common-Rail Diesel Engine. *Energy* **2023**, *278*, 127965. [CrossRef]
49. Daabo, A.M.; Mahmoud, S.; Al-Dadah, R.K.; Al Jubori, A.M.; Bhar Ennil, A. Numerical Analysis of Small Scale Axial and Radial Turbines for Solar Powered Brayton Cycle Application. *Appl. Therm. Eng.* **2017**, *120*, 672–693. [CrossRef]

Disclaimer/Publisher's Note: The statements, opinions and data contained in all publications are solely those of the individual author(s) and contributor(s) and not of MDPI and/or the editor(s). MDPI and/or the editor(s) disclaim responsibility for any injury to people or property resulting from any ideas, methods, instructions or products referred to in the content.